Catalysts **2015**, *5*, 349-365; doi:10.3390/catal5010349

OPEN ACCESS

catalysts

ISSN 2073-4344

www.mdpi.com/journal/catalysts

Article

A Mechanistic Study of Direct Activation of Allylic Alcohols in Palladium Catalyzed Amination Reactions

Yasemin Gumrukcu, Bas de Bruin * and Joost N. H. Reek *

Van 't Hoff Institute for Molecular Sciences, University of Amsterdam, Science Park 904, 1098 XH, Amsterdam, The Netherlands; E-Mail: yasmin.gumrukcu@gmail.com

* Authors to whom correspondence should be addressed; E-Mails: b.debruin@uva.nl (B.B.); j.n.h.reek@uva.nl (J.N.H.R.); Tel.: +31-20-525-6495 (B.B.); +31-20-525-5265 (J.N.H.R.); Fax: +31-20-525-5604 (B.B.); +31-20-525-5604 (J.N.H.R.).

Academic Editor: Keith Hohn

Received: 11 December 2014 / Accepted: 28 February 2015 /Published: 11 March 2015

Abstract: We here report a computational approach on the mechanism of allylicamination reactions using allyl-alcohols and amines as the substrates and phosphoramidite palladium catalyst **1a**, which operates in the presence of catalytic amount of 1,3-diethylurea as a co-catalyst. DFT calculations showed a cooperative hydrogen-bonding array between the urea moiety and the hydroxyl group of the allyl alcohol, which strengthens the hydrogen bond between the O-H moiety of the coordinated allyl-alcohol and the carbonyl-moiety of the ligand. This hydrogen bond pattern facilitates the (rate-limiting) C-O oxidative addition step and leads to lower energy isomers throughout the catalytic cycle, clarifying the role of the urea-moiety.

Keywords: amination; allylic alcohols; palladium; DFT calculations; allylic alkylation

1. Introduction

The direct activation of allylic alcohols, without pre-activation of the alcohol moiety, in palladium catalyzed allylic substitution reactions for application in C-C and C-X bond formation, is of growing interest [1–3]. Traditionally, allylic alcohols are pre-activated by transforming the alcohol moiety into a better leaving group, such as a halide, tosylate, carboxylate or phosphate. Alternatively they can be activated by stoichiometric Lewis acid adducts, such as BEt_3 and $Ti(O\text{-}i\text{-}Pr)_4$ [4–14]. However, all

these approaches lead to formation of substantial (in most cases stoichiometric) amounts of (salt) waste, which can be avoided by the direct catalytic activation of the allylic alcohol [15–19]. Ozawa and co-workers reported the first examples in which allylic alcohols were directly used as coupling partners in Pd-catalyzed allylic substitution reactions by the π-allyl palladium complexes of substituted diphosphinidenecyclobutene ligands (DPCB-Y) [15]. Mechanistic studies demonstrated that C-O bond dissociation is the rate-determining step in these reactions (proposed by Ozawa and Yoshifuji to proceed via a palladium-hydride intermediate) [20], which was later also confirmed by le Floch and co-workers on the basis of DFT calculations (invoking ammonium promoted protonation of the allyl alcohol) [21]. The theoretical study further showed that nucleophilic attack on the π-allyl complex first generates a cationic allyl amine, which assists in dissociation of the hydroxyl group in the oxidative addition step. Another prominent example was reported by Oshima and co-workers, showing that a EtOAc/H_2O biphasic system allows the *in situ* activation of allylic alcohols with tppts based Pd(0) catalyst by hydration of the alcohol moiety [22]. Several water molecules assist in delocalization of the developing negative charge in the transition state, and thus lower the activation energy according to the reported DFT calculations. Similarly, the use of methanol as a solvent in allylic alkylation reactions of simple ketones with allylic alcohols was reported to be crucial for the C-O bond cleavage step, which was catalyzed by the [(dppf)Pd(allyl)] in the presence of pyrolidine as co-catalyst [23]. Solvation of the hydroxyl/hydroxy moiety in the charge-developing transition state was again proposed to lower the activation energy.

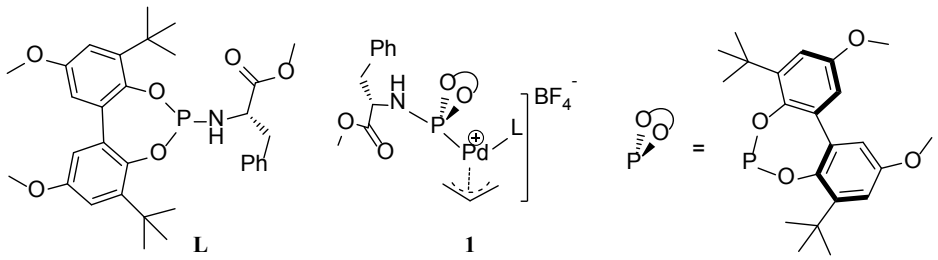

Scheme 1. The structure of phosphoramidite ligand (**L**) and schematic representation of Pd-allyl complex, **1**.

We recently disclosed a new phosphoramidite-based Pd(π-allyl)catalyst (**1**) for allylic substitution reactions, using unactivated allylic alcohols to selectively produce linear alkylated and aminated products (Scheme 1) [24]. The addition of catalytic amount of 1,3-diethylurea (3 mol%) increased the catalytic activity and improved the reproducibility of these reactions. Detailed kinetic studies revealed zero order kinetics in the nucleophilic amine and first order kinetics in the allylic alcohol and 1,3-diethylurea. On this basis, we proposed the mechanism depicted in Scheme 2. The catalyst precursor **1** was generated *in situ* by mixing [(η^3-allyl)Pd(cod)]BF_4 with ligand **L**. Nucleophilic attack of amine is expected to generate intermediate **2**, and the coordination of the allyl alcohol to palladium results in formation of intermediate **3** and the allylamine product. Experimentally, we observed product inhibition; the reaction becomes slower with increasing amounts of the product. This is most likely due to a shift in the equilibrium between intermediate **3** and **2** in favor of **2** at higher product concentrations. In line with observations reported by others, the allylic alcohol C-O bond oxidative addition step is likely the rate-determining step. Preliminary DFT calculations suggested that

hydrogen-bonding interactions between the hydroxyl group of the alcohol and both the carboxyl group of the ligand and the1,3-diethylurea moiety assist in the C-O bond activation step. Mechanistic details of the direct activation of allylic alcohols by this system, and in particular the role of the 1,3-diethylurea additive in this process, are required to facilitate further development of this type of catalyst systems. Here we report the mechanism of the Pd-catalyzed direct amination of allylic alcohols based on DFT calculations. We also found the mechanism by which the 1,3-diethylurea additive activates the catalyst as it forms H-bonds with the allylalcohol substrate.

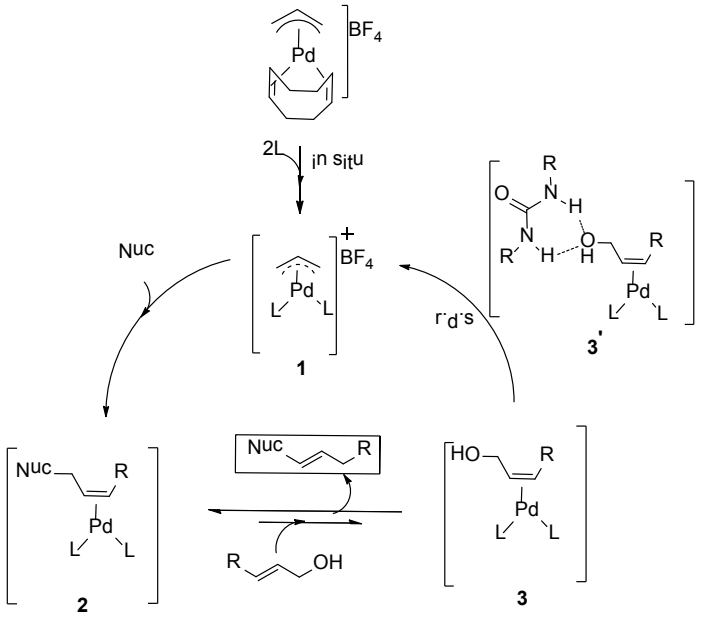

Scheme 2. Proposed mechanism for amination reactions of allylic alcohols [22].

2. Results and Discussion

The mechanism we explored computationally is based on our experimental kinetic studies (Scheme 2). The rate limiting step derived from the kinetic studies is the C-O bond oxidative addition in intermediate **3**, judging from the first order rate dependency on allyl alcohol and 1,3-diethylurea and zero order behavior in the amine (=nucleophile). We took this information as a starting point to build our computational model. For the theoretical calculations, we employed allyl alcohol and *N*-methylaniline as the substrate and nucleophile, respectively. The reaction produces the corresponding allyl-amine as the product (Scheme 2). To avoid complicated conformational searches, the ligand **L** was simplified by removing the bulky substituents of the backbone and replacing the chiral benzyl group by a methyl group (*S* chirality maintained, see **L'**, Scheme 3a). Notably, the preferred *R* chirality on bi-phenyl backbones of the phosphoramidite ligand **L** in the palladium homo-complex **1** [25] complies with the DFT calculations using the simplified ligand **L'** in **I**. Further note that the chiral element of the ligand was not used to induce enantioselectivity, neither experimentally nor in the DFT calculations. In the Figures and Schemes, ligand **L'** is drawn in a simplified manner showing only the relevant parts of the ligand for clarity (Scheme 3b). We performed all calculations in Turbomole with the BP86 functional. We employed the large def2-TZVP basis set and Grimme's version 3 (DFT-D3, disp3) dispersion corrections.

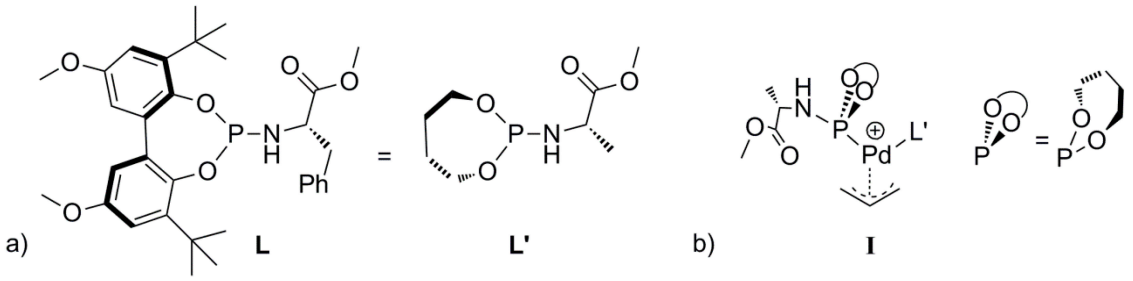

Scheme 3. (**a**) The ligand **L** and the simplified ligand **L'**. (**b**) Schematic representation of the **L'** based Pd-allyl complex **I**.

We started by optimizing the geometries of several isomers of the π-allyl complex **I** having different conformation of ligand **L'** around the metal center. In subsequent studies we took the structure with the lowest energy as the reference point ($G^0_{\mathbf{I}} = 0$ kcal mol^{-1}). The coordination geometry of the palladium center in this structure is square planar, with the P-donor of the two ligands L' and the two donor sites of the bidentate allyl-ligand surrounding the metal. The steric interactions between the two ligands L' mutually and with the allyl ligand appear to be minimized in **I** (Scheme 4). This geometry of the Pd(**L'**) moiety is used for the calculation of succeeding reaction intermediates.

First, we investigated the nucleophilic attack of the amine to the allyl moiety of complex **I**. In principle, the nucleophilic attack could follow either an inner-sphere mechanism (first coordination of the nucleophile to the metal, followed by a reductive elimination step) or outer-sphere attack (direct attack of the nucleophile to the allyl moiety, without pre-coordination of the nucleophile to the metal). This strongly depends on the basicity of amines [26,27]. Strong nucleophiles (pK_a > 20) are expected to attack the Pd metal and hence likely follow an inner-sphere mechanism while weaker nucleophiles (pK_a < 20), such as *N*-methylaniline (pK_a~10), are believed to attacked the allyl-moiety directly and likely follow an outer-sphere mechanism. Thus, in this computational study we focused on the outer-sphere mechanism.

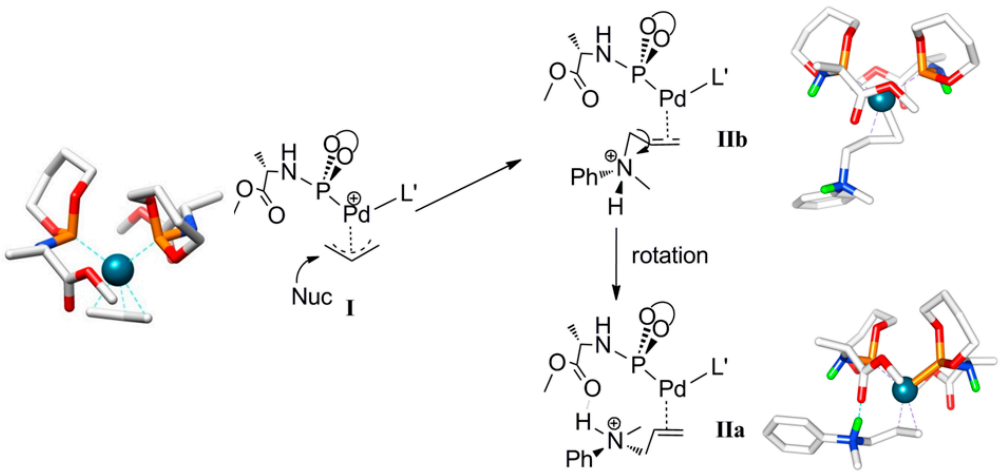

Scheme 4. Calculated structure and schematic representation of complex I, formation of complex IIbby nucleophilic attack and IIa by rotational isomerization ($\Delta G^0_{\mathbf{IIa-IIb}} = -3.5$ kcal mol^{-1}).

Outer-sphere nucleophilic attack at the allyl moiety produces the cationic Pd-allylamine complex **IIb** initially. Following this, rapid isomerization of **IIb** is expected to form the thermodynamically more stable rotamer **IIa** by C-C bond rotation (Scheme 4). The relative energies of the product **IIa** (8.2 kcal mol^{-1}) is lower than product **IIb** (11.7 kcal mol^{-1}). H-bonding between the N-H moiety of the allyl-amine and the carboxylic group of the ligand **L'** in complex **IIa** explains its relative stability (Scheme 5). Notably, the direct formation of **IIa** by the nucleophilic attack at **I** is not favorable. Steric hindrance around the palladium-allyl moiety prevents nucleophilic attack in any other direction.

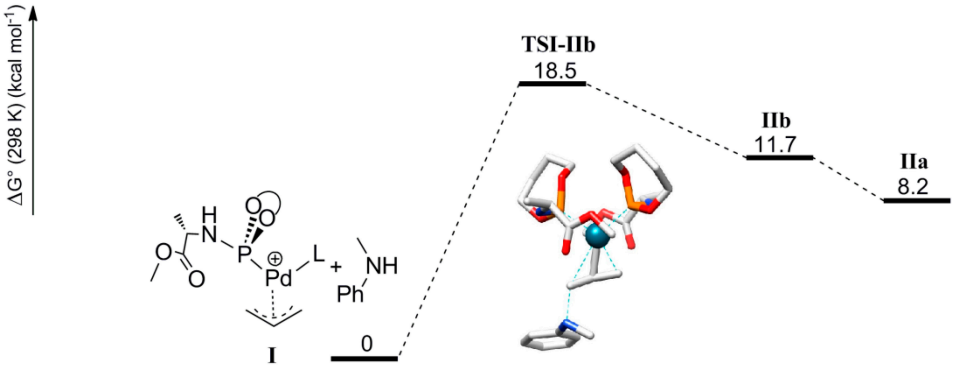

Scheme 5. Calculated pathway for nucleophilic attack of the amine at complex **I**, which forms complex **IIb**, which then converts to **IIa** via rotation (See Scheme 4 for the calculated structures and schematic representation of **IIa** and **IIb**).

In the precursor **I**, the overall positive charge is delocalized over the Pd^{II} atom, the P-donors of the ligands **L'** and the allyl moiety, while in **IIa** and **IIb** the charge is largely concentrated on the quaternary ammonium moieties. Hence, in the absence of stabilization by discrete solvent (or more likely substrate alcohol) molecules, the complexes **IIa** and **IIb** are artificially destabilized in the applied gas phase DFT calculations. However, when we applied cosmo dielectric solvent corrections, the effects of H-bonding in stabilization of some of the intermediates was partially lost due to overcompensation of dielectric forces [28], which does not represent the known effects of H-bonding in apolar solvents used experimentally. Thus, despite the abovementioned problems with charge relocation for some steps in this study, we still decided to focus mostly on a description of the mechanistic pathways on the basis of pure gas phase DFT calculations. The cosmo corrected pathways are, however, reported in the supporting information and in Scheme 8 for comparison, and we will further debate the effects of cosmo corrections in the discussion about the rate limiting step of the catalytic cycle (*vide infra*). The overestimated entropies in the gas phase as compared to solution data were corrected by the suggested 6 kcal mol^{-1} correction term for each step involving a change in the number of species (see experimental section for details).

The second step considered in the DFT computed mechanism is the displacement of the protonated allyl-amine coordinated to Pd^0 by the allyl-alcohol substrate (Scheme 6). Since gas phase DFT calculations become very unreliable when complete charge changes of the computed molecules are involved (e.g., converting a cationic species to a neutral species), we treated this step by keeping the cationic ammonium product H-bonded to the coordinated allyl alcohol. Furthermore, in previous studies, similar treatments (again to avoid charge-associated problems in gas phase calculations) were

found to actually have a barrier-lowering effect on the subsequent oxidative addition step due to H-bond assisted C-O bond breaking [19]. The coordination of the allyl alcohol substrate to Pd^0 can occur in two manners, leading to two possible configurations **IVa** and **IVb** based on the position of the hydroxyl group with respect to the carboxyl group of ligand **L'**. In **IVa** the hydroxyl group of the allylalcohol is H-bonded to the carbonyl group of **L'**, whereas in **IVb** it is not. In both cases the protonated allylamine is H-bonded to the oxygen atom of the hydroxyl group of the Pd coordinated allyl-alcohol substrate (Scheme 6). The computed relative free energies of **IVa** and **IVb** (relative to precursor **I**) are –0.3 and 6.1 kcal mol^{-1}, respectively. Hence species **IVa** is the most stable intermediate. Complex **IVa** might also form via rotational isomerization of **IVb**.

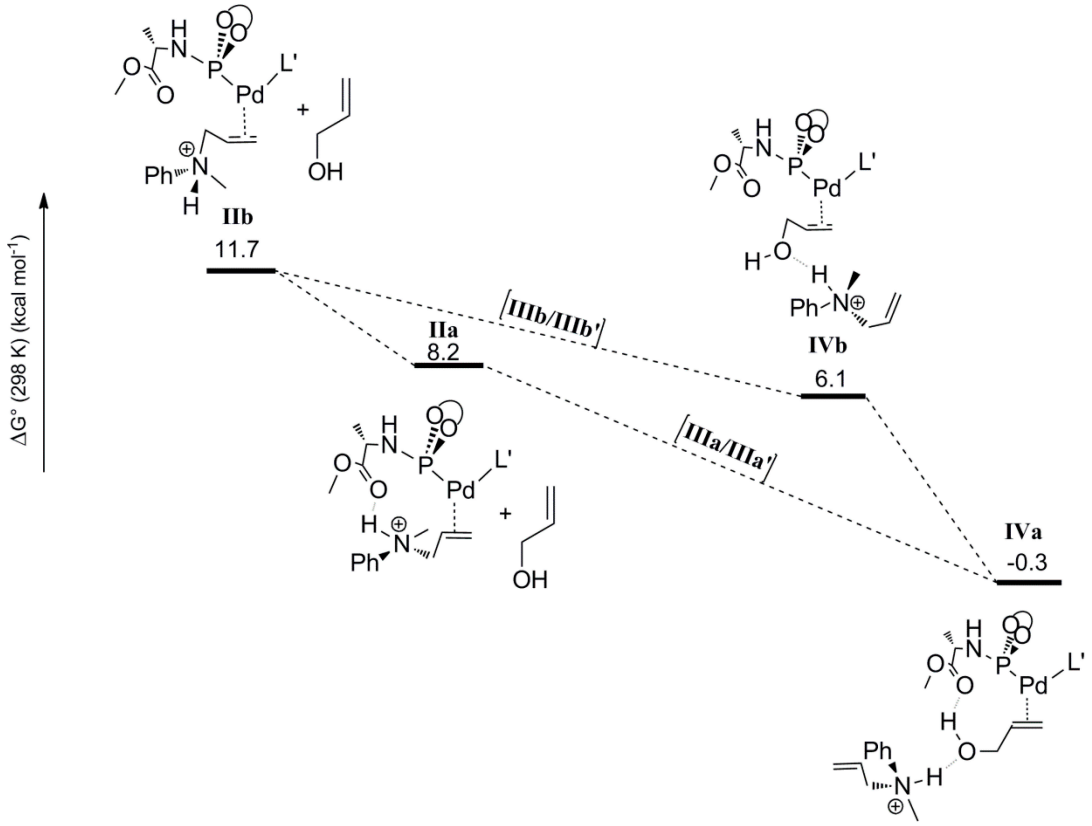

Scheme 6. Substitution of the coordinated allyl-ammonium product by the allyl alcohol substrate leading to species **IVa** and **IVb**.

To elucidate the possible role of the 1,3-diethylurea moiety, we also optimized the geometries **IIIa** and **IIIb**, which are analogues of **IVa** and **IVb** lacking the H-bonded allyl-ammonium moiety. The energies and geometries of **IIIa** and **IIIb** were compared to their analogues **IIIa'** and **IIIb'**, each containing a 1,3-diethylurea moiety double H-bonded to the hydroxyl of the coordinated allyl-alcohol (Scheme 7). Complex **IIIa** is more stable than **IIIb** (relative energies 0 and 3.5 kcal mol^{-1}, respectively), in line with the fact that **IIIb** lacks the internal hydrogen bonding between the hydroxyl moiety of the allylalcohol and the carboxyl group of **L'**. The hydrogen bonded 1,3-diethylurea moiety further stabilizes **IIIa'** substantially (ΔG^0 = −15.9 kcal mol^{-1}) whereas species **IIIb'** shows less stabilization (ΔG^0 = −7.4 kcal mol^{-1}). Hence, the H-bonding pattern in **IIIa'** based on internal H-bond donation from the hydroxyl-group to ligand **L'** and hydrogen bond acceptation from the

1,3-diethylurea H-bond donor is clearly cooperative, a feature that is commonly observed and is a consequence of polarization. It is very likely that this also plays an important role in the oxidative addition process under the experimental conditions. Unfortunately, it was not possible to compute the effect of 1,3-diethyl urea H-bonding on the barrier of the rate determining oxidative addition process. This is due to the abovementioned requirement to keep the overall charge neutral to prevent any unrealistic charge effects in the gas phase calculations. Hence, to still mimic the effect of a hydrogen bond, we used the associated allyl-ammonium salt product, which can deliver a proton after the transition state to keep an overall 1+ charge for each complex involved in that catalytic cycle.

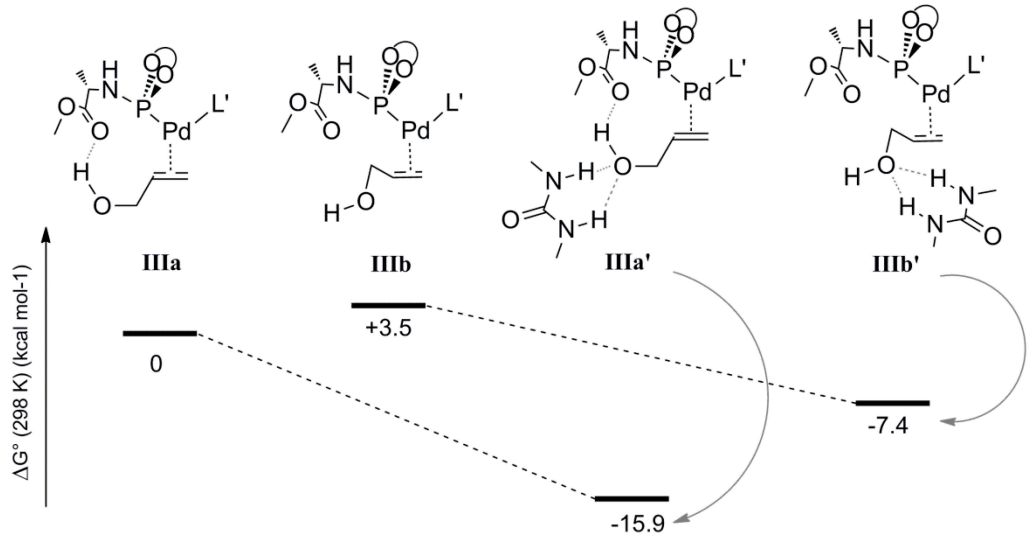

Scheme 7. The energy profile of the allyl alcohol coordinated Pd complexes in the presence and absence of urea molecule, **IIIa-IIIa'** and **IIIb-IIIb**'.

The last step of the computed catalytic cycle involves oxidative addition of the C-O bond of the allyl alcohol substrate in intermediates **IVa** and **IVb** to regenerate the palladium-allyl intermediate **I**. Since this process involves breaking the C-O bond and liberation of a hydroxide (OH^-) moiety being a poor leaving group, this process is expected to be facilitated by hydrogen bonding. In good agreement, the **TSIVa-I** barrier (9.5 kcal mol^{-1}) for oxidative addition of the C-O bond is lower than **TSIVb-I** (15.3 kcal mol^{-1}) reflecting the effects of cooperative H-bonding (Scheme 8). The process leads to elimination of water, because the H-bonded ammonium salt transfers its proton to the hydroxide-leaving group in a concerted manner. Hence, unfavorable uncompensated charge relocations in the gas phase calculations play a smaller role in the transition states **TSIVa-I** and **TSIVb-I** than in the precursors **IVa** and **IVb**. Besides, the relative barriers on going from **IVa** and **IVb** to **TSIVa-I** and **TSIVb-I** are likely somewhat underestimated, while the absolute barriers of **TSIVa-I** and **TSIVb-I** *versus* **I** suffer less from such uncompensated charge relocation effects.

In the gas phase calculations without cosmo dielectric solvent corrections, the transition state barrier for nucleophilic attack of the amine at the allyl moiety (**TSI-IIb** = 18.5 kcal mol^{-1}) is much higher than the transition state for the oxidative addition step (**TSIVa-I** = 9.5 kcal mol^{-1}), which would indicate that the former should be the rate determining step. However, the experimental kinetic experiments clearly indicate that the oxidative addition is rate determining. Concerning the rate determining step, the experimental data and the computational model without cosmo corrections are therefore not in

agreement. This is due to the abovementioned charge concentration effects in this reaction, so that the gas phase DFT numbers do not accurately describe the solution data. Therefore we also investigated the overall pathway including cosmo dielectric solvent corrections. The results taking toluene as the medium are shown in the bottom part of Scheme 8. Indeed, this leads to a shift in the rate-limiting step from the nucleophilic attack to the oxidative addition step, in good agreement with the experimental data. To describe the effects of H-bonding, however, some of the steps seem to be better described without cosmo, which is the reason we focused on discussing those calculations first.

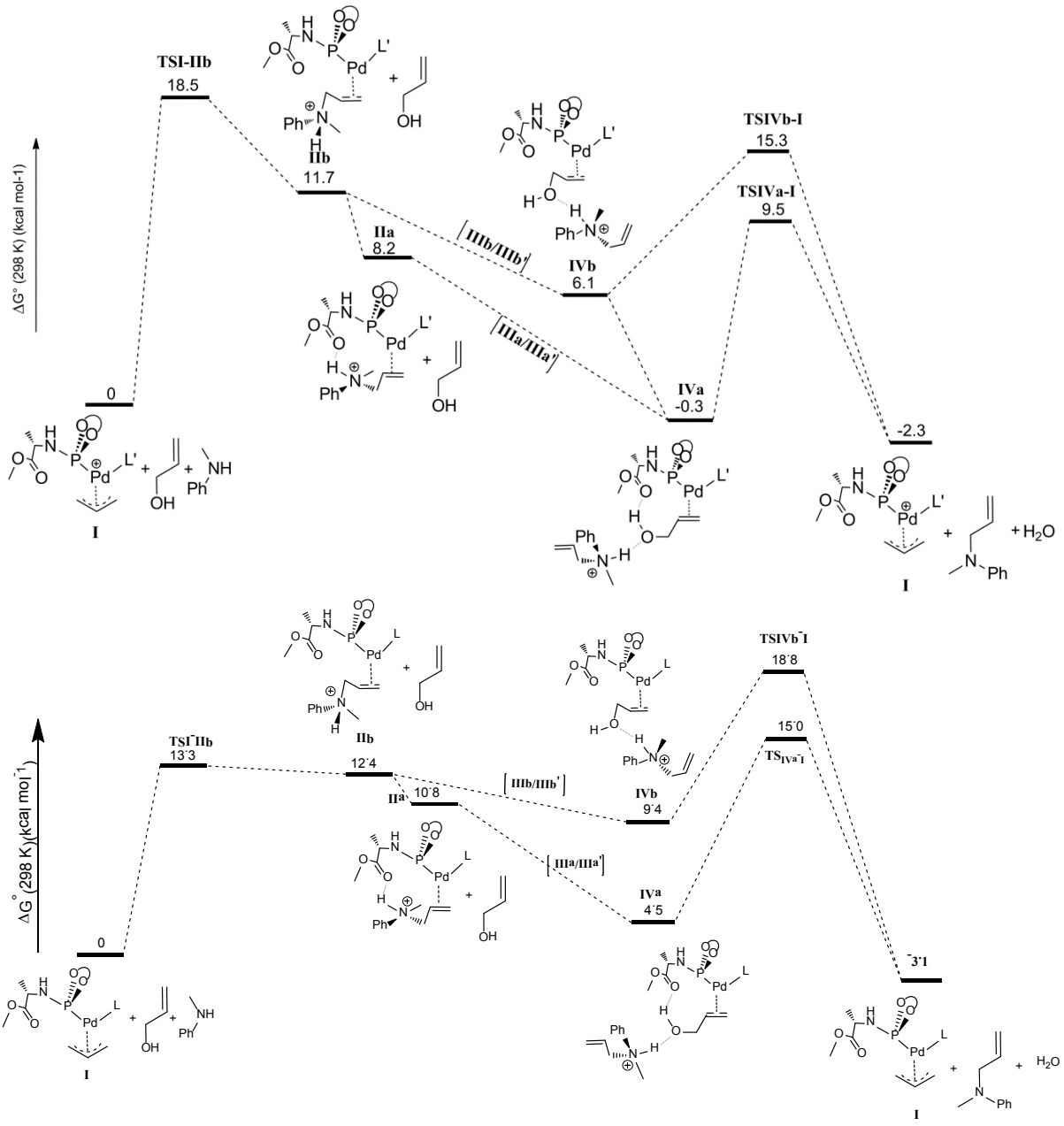

Scheme 8. Calculated catalytic pathway of the complete cycle. **Top**: Free energies without cosmo corrections; **Bottom**: Free energies with cosmo corrections (ε = 2.38; toluene).

As reported, we have discovered by kinetic analysis that product inhibition takes place during the catalysis. The coordination of the allylamine to Pd is computed to be more favorable than coordination

of the allyl alcohol. We have examined this by calculating the product coordinated Pd complexes with two possible configurations and determined the relative energies with respect to allyl alcohol coordinated Pd complexes **IIIa** and **IIIb** (Scheme 9). The formation of these complexes is expected to take place along with the formation of isomers **IVa** and **IVb** (the hydrogen bonded analogues) from **IIa** and **IIb**, which represent the product-coordinated complexes. Deprotonation of the product in complex **IIa/IIb** affords complexes **Va** and **Vb**.

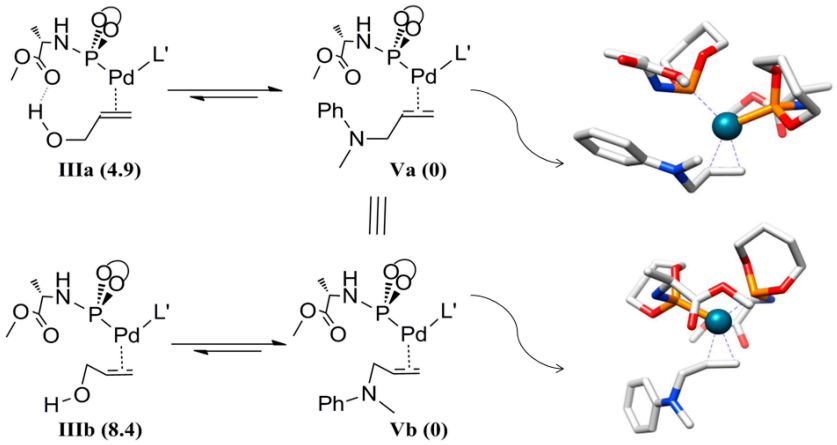

Scheme 9. Schematic representation of the product inhibition equilibriums and calculated structures of **Va** and **Vb**. The values between parentheses are the relative energies (kcal mol^{-1}). The orientation of the allylamine at Pd does not lead to a significant energy difference (complex **Va** and **Vb** have the same relative free energy).

Notably, both isomers **Va** and **Vb** have the same relative free energy, indicating the poor secondary interaction between the product and the complex, besides the alkene coordination energy. The relative energies of **IIIa** and **IIIb** with respect to **V** were found to be 4.9 and 8.4 kcal mol^{-1}, respectively. Note that the allyl amine adducts **Va** and **Vb** are more stable than the allyl alcohol adducts, in agreement with the experimental observations, showing product inhibition. This is likely due to sigma bond inductive effects of nitrogen *versus* oxygen. The lower energy of **IIIa** compared to **IIIb** is due to the hydrogen bond with the carbonyl of the ligand. The same trend is observed for intermediate **IVa** being lower in energy than the **IVb**, and the larger difference in these complexes is again a result of cooperative hydrogen bonding.

2.1. Summary of the DFT Computed Pathway

The most interesting finding of the DFT study is the cooperative hydrogen bond between the hydroxyl and carbonyl groups (substrate-ligand) and urea (or the ammonium salt we used as a reference). We found experimentally that phosphoramidite ligands that do not have the ester functionality did not show the urea co-catalyzed activation of allyl alcohols, which is in line with the DFT calculations. The interaction between the coordinated allyl alcohol and ligand **L'** proved to be significant in the whole catalytic cycle, overall lowering the relative free energy of the Pd-intermediates (Scheme 8). The function of 1,3-diethylurea is determined to further lower the barrier for C-O oxidative addition (Scheme 10a). In addition, the calculations show a preference for the

coordination of the product leading to product inhibition, however, a cooperative urea binding to **IIIa** will shift the equilibrium in favor of the substrate complex (Schemes 7 and 9). The computed catalytic cycle complies with the experimental kinetic data if we include cosmo dielectric solvent corrections. Oxidative addition of the C-O bond of the coordinated allyl alcohol in intermediate **IVa** via the rate limiting transition state **TSIVa-I** is assisted by H-bonding. This was computed using the ammonium product as the model (to reduce undesired effects of charge changes), but in practice this does explain the rate enhancing effect of the urea (Scheme 10b). This mechanism deviates from the mechanism proposed by Ozama, Samec and ourself involving allyl alcohol activation with palladium hydrides [29,30].

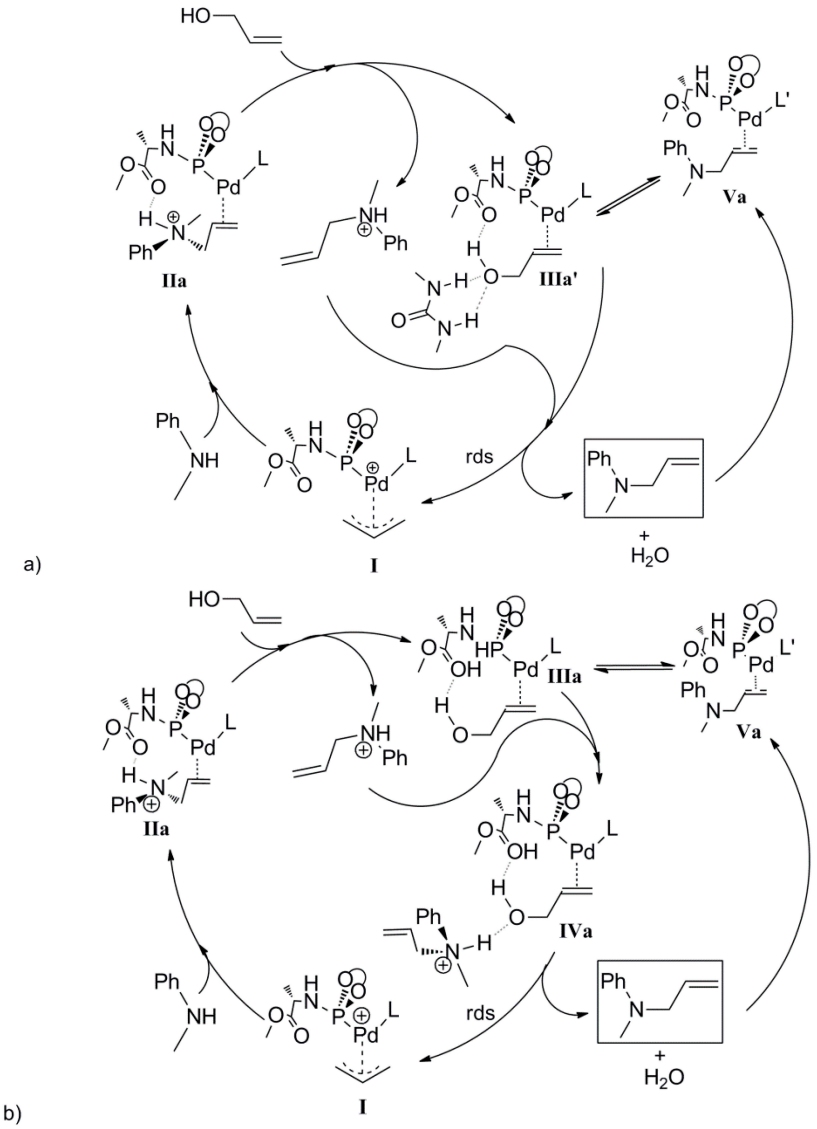

Scheme 10. (**a**) Proposed catalytic cycle in agreement with the experimental studies. (**b**) DFT calculated catalytic cycle using the allyl ammonium product as a model for urea H-bonding (intermediate IVa as a model for IIIa').

2.2. Bond Length Analysis

We analyzed the bond length changes throughout the calculated catalytic pathway in order to obtain more information about the effect of H-bond interactions on the formation of the isomeric intermediates *a* and *b* (see Table 1). First, we examined the nucleophilic attack of the *N*-methylaniline to complex **I**, which involves intermediates **IIb** and its respective transition state structure **TSI-IIb** (Figure 1). The Pd-P1 and Pd-P2 bond lengths show only small changes on going from the precursor **I** to the transition state **TSI-IIb** and subsequently formed the **IIb**, which has virtually same bond distances as **I** (Table 1).

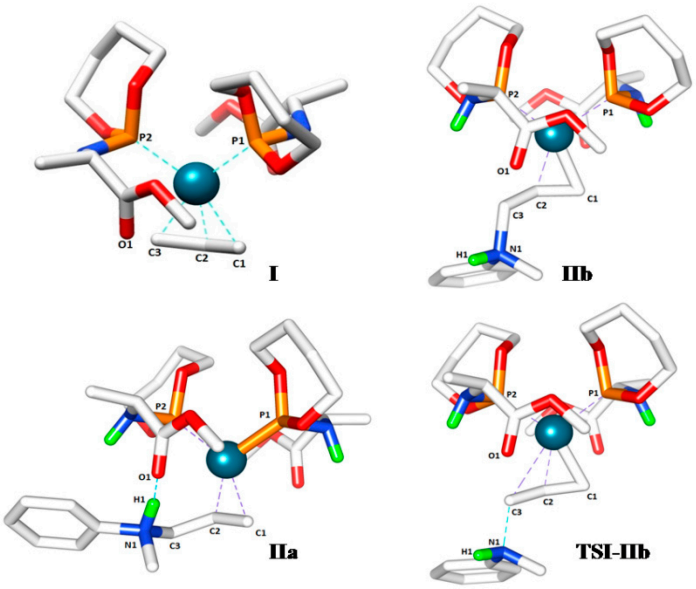

Figure 1. In all structures the related atoms are labeled such that C1 refers to the allyl carbon trans to P2, C2 is the central allyl carbon and C3 is the terminal allyl carbon trans to P1.

Table 1. Bond lengths (Å) of the calculated structures of intermediates involved in nucleophilic attack.

Bond	I	IIa	IIb	TSI-IIb
*d*Pd-P1	2.261	2.274	2.261	2.256
*d*Pd-P2	2.262	2.245	2.26	2.266
*d*Pd-C1	2.233	2.176	2.143	2.147
*d*Pd-C2	2.205	2.149	2.162	2.176
*d*Pd-C3	2.225	3.167	2.99	2.853
*d*C3-N1	-	1.521	1.639	1.841
*d*N1-H1	-	1.054	1.028	1.025
*d*H1-O1	-	1.8	-	-

The attack of the amine leads to elongation of the Pd-C3 bond (**I** Pd-C3 = 2.225 Å, **TSI-IIb** Pd-C3 = 2.853 Å) while the Pd-C1 and Pd-C2 bonds shorten, as expected. On the other hand, generated by the rotational isomerization, the coordinated ligands of **IIa** require a rearrangement of the ligands around palladium to allow the H-bond interactions between the proton of the amine (H1) and the carboxyl moiety of the ligand (O1). Thus, the bond lengths of Pd-P1 and Pd-P2 show clear changes

(compare Pd-P1 = 2.261 Å, Pd-P2 = 2.260 Å in **IIb** with Pd-P1 = 2.274 Å, Pd-P2 = 2.245 Å in **IIa**) (Table 1). Besides, the newly formed C3-N1 bond is also affected by the H-bond interactions. The shorter C3-N1 bond of the lower energy isomer **IIa** must be the result of H1-O1 interaction as it directs the positioning of the amine (**IIa** C3-N1 = 1.521 Å, **IIb** C3-N1 = 1.639 Å) (Table 1).

Next, we analysed the bond length changes occurring in the oxidative addition step, which involves the simultaneous carbon-hydroxyl bond dissociation (C3-O2), hydroxyl-hydrogen bond formation (H1-O2, water), the release of the product and formation of the complex **I** (Table 2). The intermediate **IVa** was found lowest in energy (−0.3 kcal mol^{-1}), which also needed lower activation energy than **IVb** to generate the products (**TSIVa-I** = 9.5 and **TSIVa-I** = 15.3 kcal mol^{-1}). Judging from the comparative Pd-C3 distances of **TSIVa-I** and **TSIVb-I** (3.223 and 2.816 Å, respectively) relative to **I** (2.225 Å), the **TSIVa-I** represents an early transition state (Table 2). Moreover, we determined that the additional H-bond interaction in **TSIVa-I**, between the proton acceptor carbonyl (O1) and proton donor hydroxyl group (H2), facilitates the C3-O2, N1-H1 bond dissociation and H1-O2 bond formation processes of the transition state by altering the partial charges of the participating atoms (Figure 2). The C3-O2 and N1-H1 bonds are longer in **TSIVa-I** (1.950 and 1.760 Å) compared to **TSIVb-I** (1.844 and 1.360Å) and the H1-O2 bond distance in **TSIVa-I** (1.018 Å) is shorter than in **TSIVb-I** (1.171 Å), which might be the effect of complementary H-bonding in **TSIVa-I**.

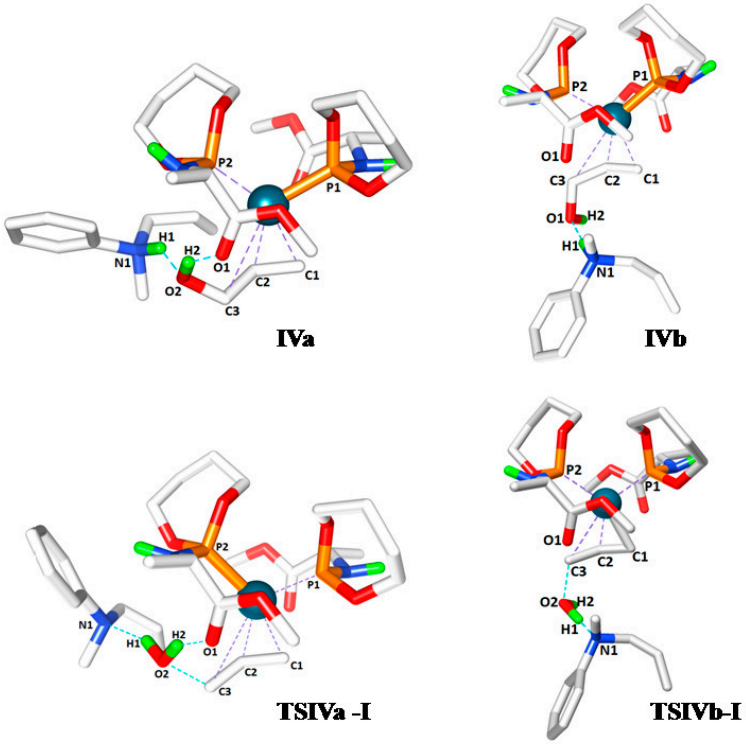

Figure 2. Transition state structures of **IVa**, **TSIVa-I**, **IVb** and **TSIVb-I**.

Table 2. Bond lengths (Å) of the calculated structures of intermediates involved in oxidative addition step.

Bond	I	IVa	IVb	TSIVa-I	TSIVb-I
*d*Pd-P1	2.261	2.272	2.259	2.244	2.26
*d*Pd-P2	2.262	2.235	2.247	2.284	2.271
*d*Pd-C1	2.233	2.218	2.167	2.128	2.143
*d*Pd-C2	2.205	2.261	2.158	2.334	2.199
*d*Pd-C3	2.225	3.182	3.048	3.223	2.816
*d*C3-O2	-	1.454	1.501	1.950	1.844
*d*N1-H1	-	1.064	1.081	1.760	1.360
*d*H1-O2	-	1.793	1.575	1.018	1.171
*d*H2-O2	-	0.988	0.975	0.997	0.976
*d*H2-O1	-	1.845	-	1.720	-

3. Experimental Section

Computational Details. Geometry optimizations were carried out with the Turbomole program package [31] coupled to the PQS Baker optimizer [32] via the BOpt package [33], at the ri-DFT level using the BP86 [34,35] function and the resolution-of-identity (ri) method [36]. We optimized the geometries of all stationary points at the def2-TZVP basis set level [37], employing Grimme's dispersion corrections (DFT-D3, disp3 version) [38]. The identity of the transition states was confirmed by following the imaginary frequency in both directions (IRC). All minima (no imaginary frequencies) and transition states (one imaginary frequency) were characterized by calculating the Hessian matrix. ZPE and gas-phase thermal corrections (entropy and enthalpy, 298 K, 1 bar) from these analyses were calculated. The relative free energies obtained from these calculations are reported in the Schemes and Figures of this chapter.

By calculation of the partition function of the molecules in the gas phase, the entropy of dissociation or coordination for reactions in solution is overestimated (overestimated translational entropy terms in the gas phase compared to solutions). For reactions in "solution", we therefore corrected the Gibbs free energies for all steps involving a change in the number of species. Several methods have been proposed for corrections of gas phase to solution phase data. The minimal correction term is a correction for the condensed phase (CP) reference volume (1 L mol^{-1}) compared to the gas phase (GP) reference volume (24.5 L mol^{-1}). This leads to an entropy correction term (SCP = SGP + Rln{1/24.5} for all species, affecting relative free energies (298 K) of all associative steps of −2.5 kcal mol^{-1} [39]. Larger correction terms of −6.0 kcal mol^{-1} have been suggested based on solid arguments [40,41]. While it remains a bit debatable which entropy correction term is best to translate gas phase DFT data into free energies relevant for reactions in solution, in this chapter we adapted the suggested correction term of −6.0 kcal mol^{-1} [40,41]. Separately, additional dielectric constant corrections (comso [42]) were taken into account with single point calculations, using the dielectric constants of toluene (ε = 2.38), ethylacetate (ε = 6.02) and water (ε = 78.54). The cosmo corrected energy pathways are shown in the supporting information and in Scheme 8.

4. Conclusions

We studied by DFT calculations the mechanistic pathway of the amination reaction of allylic alcohols using catalyst **1**, which operates in the presence of catalytic amount of 1,3-diethylurea as a co-catalyst. The DFT calculation without cosmo dielectric solvent corrections predict the nucleophilic attack of the amine to be rate determining, while experimentally the oxidative addition step was found to be the rate-determining step. However, when including cosmo corrections, the DFT model is in good agreement with the experimental kinetic data. Yet, some steps in the catalytic cycle, which involve effects of H-bonding, seem to be better described without cosmo corrections. Notably, the operation mode of the urea additive in the overall mechanism of the catalytic reaction has become clear. The urea moiety hydrogen bonds to the hydroxyl of the allyl alcohol, which in turn hydrogen bonds to the carbonyl of the ligand. The hydrogen bonding is cooperative, most likely because of polarization effects. The hydrogen bonds are present throughout the cycle, including the transition state for oxidative addition (**TSIVa-I**). Clearly, in this transition state, the hydrogen bond leads to a lower energy compared to the non-hydrogen bonded analogue **IVb**. The oxidative addition process from **IVa** was computed to be exergonic, affording the aminated product, water and regenerating the allyl form of the catalyst (**I**). The effect of the H-bonding pattern is reflected by insignificant different bond length changes for the pathways with and without H-bonding, both in the nucleophilic attack of the amine on the allyl moiety and on the C-O oxidative addition step. In all cases, the hydrogen bond interaction leads to lower energy isomers. Concisely, H-bonding between the carboxyl group of the ligand **L'** and the protons of the coordinated allyl amine or alcohol, **IIa** or **IVa** leads to lower energy isomers with lower barriers throughout the catalytic cycle.

Acknowledgments

This research has been performed within the framework of the CatchBio program. The authors gratefully acknowledge the support of the Smart Mix Program of the Netherlands Ministry of Economic Affairs and the Netherlands Ministry of Education, Culture and Science.

Author Contributions

Yasemin Gumrukcu performed the DFT calculations with help and supervision provided by Bas de Bruin and Joost Reek. The paper was written by all three authors.

Conflicts of Interest

The authors declare no conflict of interest.

References

1. Yamamoto, T.; Akimoto, M.; Saito, O.; Yamamoto, A. Interaction of palladium(0) complexes with allylic acetates, allyl ethers, allyl phenyl chalcogenides, allylic alcohols, and allylamines. Oxidative addition, condensation, disproportionation, and π-complex formation. *Organometallics* **1986**, *5*, 1559–1567.

2. Sundararaju, B.; Achard, M.; Bruneau, C. Transition metal catalyzed nucleophilic allylic substitution: activation of allylic alcohols via π-allylic species. *Chem. Soc. Rev*. **2012**, *41*, 4467–4483.
3. Kayaki, Y.; Koda, T.; Ikariya, T. Halide-Free Dehydrative Allylation Using Allylic Alcohols Promoted by a Palladium−Triphenyl Phosphite Catalyst. *J. Org. Chem.* **2004**, *69*, 2595–2597.
4. Trost, B.M.; van Vranken, D.L. Asymmetric transition metal-catalyzedallylicalkylations. *Chem. Rev*. **1996**, *96*, 395–422.
5. Kimura, M.; Tomizawa, T.; Horino, Y.; Tanaka, S.; Tamaru, Y. Et_3B-Pd-promoted allylation of benzaldehyde with allylic alcohols. *Tetrahedron Lett.* **2000**, *41*, 3627–3629.
6. Kimura, M.; Horino, Y.; Mukai, R.; Tanaka, S.; Tamaru, Y. Strikingly Simple Direct α-Allylation of Aldehydes with Allyl Alcohols: Remarkable Advance in the Tsuji−Trost Reaction. *J. Am. Chem. Soc.* **2001**, *123*, 10401–10402.
7. Kimura, M.; Futamata, M.; Shibata, K.; Tamaru, Y. Pd-Et_3B-catalyzed alkylation of amines with allylic alcohols. *Chem. Commun.* **2003**, 234–235.
8. Kimura, M.; Futamata, M.; Mukai, R.; Tamaru, Y. Pd-Catalyzed C_3-Selective Allylation of Indoles with Allyl Alcohols Promoted by Triethylborane. *J. Am. Chem. Soc.* **2005**, *127*, 4592–4593.
9. Trost, B.M.; Quancard, J. Palladium-Catalyzed Enantioselective C-3 Allylation of 3-Substituted-1*H*-Indoles Using Trialkylboranes. *J. Am. Chem. Soc.* **2006**, *128*, 6314–6315.
10. Itoh, K.; Hamaguchi, N.; Miura, M.; Nomura, M. Palladium-catalysed reaction of aryl-substituted allylic alcohols with zinc enolates of β-dicarbonyl compounds in the presence of titanium(IV) isopropoxide. *J. Chem. Soc. Perkin Trans.* **1992**, *1*, 2833–2835.
11. Satoh, T.; Ikeda, M.; Miura, M.; Nomura, M. Palladium-Catalyzed Etherification of Allyl Alcohols Using Phenols in the Presence of Titanium(IV) Isopropoxide. *J. Org. Chem.* **1997**, *62*, 4877–4879.
12. Yang, S.C.; Hung, C.W. Palladium-Catalyzed Amination of Allylic Alcohols Using Anilines. *J. Org. Chem.* **1999**, *64*, 5000–5001.
13. Yang, S.C.; Tsai, Y.C.; Shue, Y.J. Direct Platinum-Catalyzed Allylation of Anilines Using Allylic Alcohols. *Organometallics* **2001**, *20*, 5326–5330.
14. Shue, Y.J.; Yang, S.C.; Lai, H.C. Direct palladium(0)-catalyzed amination of allylic alcohols with aminonaphthalenes. *Tetrahedron Lett.* **2003**, *44*, 1481–1485.
15. Ozawa, F.; Okamoto, H.; Kawagishi, S.; Yamamoto, S.; Minami, T.; Yoshifuji, M. (π-Allyl)palladium Complexes Bearing Diphosphinidenecyclobutene Ligands (DPCB): Highly Active Catalysts for Direct Conversion of Allylic Alcohols. *J. Am. Chem. Soc.* **2002**, *124*, 10968–10969.
16. Banerjee, D.; Jagadeesh, R.V.; Junge, K.; Junge, H.; Beller, M. An Efficient and Convenient Palladium Catalyst System for the Synthesis of Amines from Allylic Alcohols. *ChemSusChem* **2012**, *5*, 2039–2044.
17. Banerjee, D.; Jagadeesh, R.V.; Junge, K.; Junge, H.; Beller, M. Efficient and Convenient Palladium-CatalyzedAmination of Allylic Alcohols with *N*-Heterocycles. *Angew. Chem. Int. Ed*. **2012**, *51*, 11556–11560.

18. Hsu, Yi-C.; Gan, K.H.; Yang, S.C. Palladium-catalyzed allylation of acidic and less nucleophilic anilines using allylic alcohols directly. *Chem. Pharm. Bull*. **2005**, *53*, 1266–1269.
19. Ghosh, R.; Sarkar, A. Palladium-Catalyzed Amination of Allyl Alcohols. *J. Org. Chem.* **2011**, *76*, 8508–8512.
20. Ozawa, F.; Ishiyama, T.; Yamamoto, S.; Kawagishi, S.; Murakami, H. Catalytic C−O Bond Cleavage of Allylic Alcohols Using Diphosphinidenecyclobutene-Coordinated Palladium Complexes: A Mechanistic Study. *Organometallics* **2004**, *23*, 1698–1707.
21. Piechaczyk, O.; Thoumazet, C.; Jean, Y.; le Floch, P. DFT Study on the Palladium-Catalyzed Allylation of Primary Amines by Allylic Alcohol. *J. Am. Chem. Soc.* **2006**, *128*, 14306–14317.
22. Kinoshita, H.; Shinokubo, H.; Oshima, K. Water Enables Direct Use of Allyl Alcohol for Tsuji-Trost Reaction without Activators. *Org. Lett.* **2004**, *6*, 4085–4088.
23. Huo, X.; Yang, G.; Liu, D.; Liu, Y.; Gridnev, I.D.; Zhang, W. Palladium-Catalyzed Allylic Alkylation of Simple Ketones with Allylic Alcohols and Its Mechanistic Study. *Angew. Chem. Int. Ed*. **2014**, *53*, 6776–6780.
24. Gumrukcu, Y.; de Bruin, B.; Reek, J.N.H. Hydrogen-Bond-Assisted Activation of Allylic Alcohols for Palladium-Catalyzed Coupling Reactions. *ChemSusChem* **2014**, *7*, 890–896.
25. The bi-phenyl backbone of the phosphoramidite ligand **L** in the palladium homocomplex **1** has a prevalent *R* configuration that we determined by CD and VT-NMR spectroscopy.
26. Muzart, J. Procedures for and Possible Mechanisms of Pd-Catalyzed Allylations of Primary and Secondary Amines with Allylic Alcohols. *Eur. J. Org. Chem*. **2007**, *19*, 3077–3089.
27. Comas-Vives, A.; Stirling, A.; Lledos, A.; Ujaque, G. The Wacker Process: Inner- or Outer-Sphere Nucleophilic Addition? New Insights from *Ab Initio* Molecular Dynamics. *Chem. Eur. J.* **2010**, *16*, 8738–8747.
28. Aquino, A.J.A.; Tunega, D.; Haberhauer, G.; Gerzabek, M.H.; Lischka, H. Solvent Effects on Hydrogen Bonds. A Theoretical Study. *J. Phys. Chem. A* **2002**, *106*, 1862–1871.
29. Sawadjoon, S.; Sjöberg, P.J. R.; Orthaber, A.; Matsson, O.; Samec, J.S.M. Mechanistic Insights into the Pd-Catalyzed Direct Amination of Allyl Alcohols: Evidence for an Outer-Sphere Mechanism Involving a Palladium Hydride Intermediate. *Chem. Eur. J.* **2014**, *20*, 1520–1524.
30. Gumrukcu, Y.; de Bruin, B.; Reek, J.N.H. Dehydrative cross-coupling reactions of allylic alcohols with olefins. *Chem. Eur. J.* **2014**, *20*, 10905–10909.
31. Ahlrichs, R. *Turbomole Version 6.4*; University of Karlsruhe: Germany, 2012.
32. Baker, I. An algorithm for the location of transition states. *J. Comput. Chem.* **1986**, *7*, 385–395.
33. Budzelaar, P.H.M. Geometry optimization using generalized, chemically meaningful constraints *J. Comput. Chem*. **2007**, *28*, 2226–2236.
34. Becke, A.D. Density-functional exchange-energy approximation with correct asymptotic behavior. *Phys. Rev. A* **1988**, *38*, 3098–3100.
35. Perdew, J.P. Density-functional approximation for the correlation energy of the inhomogeneous electron gas. *Phys. Rev. B* **1986**, *33*, 8822.
36. Sierka, M.; Hogekamp, A.; Ahlrichs, R. Fast evaluation of the Coulomb potential for electron densities using multipole accelerated resolution of identity approximation. *J. Chem. Phys.* **2003**, *118*, 9136–9148.

37. Schaefer, A.; Horn, H.; Ahlrichs, R. Fully optimized contracted Gaussian basis sets for atoms Li to Kr. *J. Chem. Phys*. **1992**, *97*, 2571–2577.
38. Grimme, S.; Antony, J.; Ehrlich, S.; Krieg, H. A consistent and accurate *ab initio* parametrization of density functional dispersion correction (DFT-D) for the 94 elements H-Pu. *J. Chem. Phys.* **2010**, *132*, 154104–154119.
39. Dzik, W.I.; Xu, X.; Zhang, X.P.; Reek, J.N. H.; de Bruin, B. 'Carbene Radicals' in Co^{II}(por)-Catalyzed Olefin Cyclopropanation. *J. Am. Chem. Soc.* **2010**, *132*, 10891–10902.
40. Wertz, D.H. Relationship between the gas-phase entropies of molecules and their entropies of solvation in water and 1-octanol. *J. Am. Chem. Soc.***1980**, *102*, 5316–5322.
41. Schneider, N.; Finger, M.; Haferkemper, C.; Bellemin-Laponnaz, S.; Hofmann, P.; Gade, L. Metal Silylenes Generated by Double Silicon-Hydrogen Activation: Key Intermediates in the Rhodium-Catalyzed Hydrosilylation of Ketones. *Angew. Chem. Int. Ed.* **2009**, *48*, 1609–1613.
42. Klamt, A.; Schüürmann, G. COSMO: A new approach to dielectric screening in solvents with explicit expressions for the screening energy and its gradient. *J. Chem. Soc. Perkin Trans.* **1993**, *2*, 799–805.